

---

# TOWARDS ACCURATE STATE ESTIMATION: KALMAN FILTER INCORPORATING MOTION DYNAMICS FOR 3D MULTI-OBJECT TRACKING

---

**Mohamed Nagy**

Electrical and Computer Engineering  
Khalifa University  
mohamed.nagy@ieee.org

**Naoufel Werghi**

Electrical and Computer Engineering  
Khalifa University  
naoufel.werghi@ku.ac.ae

**Bilal Hassan**

Electrical and Computer Engineering  
Khalifa University  
bilal.hassan@ku.ac.ae

**Jorge Dias**

Electrical and Computer Engineering  
Khalifa University  
jorge.dias@ku.ac.ae

**Majid Khonji**

Electrical and Computer Engineering  
Khalifa University  
majid.khonji@ku.ac.ae

May 13, 2025

## ABSTRACT

This work addresses the critical lack of precision in state estimation in the Kalman filter for 3D multi-object tracking (MOT) and the ongoing challenge of selecting the appropriate motion model. Existing literature commonly relies on constant motion models for estimating the states of objects, neglecting the complex motion dynamics unique to each object. Consequently, trajectory division and imprecise object localization arise, especially under occlusion conditions. The core of these challenges lies in the limitations of the current Kalman filter formulation, which fails to account for the variability of motion dynamics as objects navigate their environments. This work introduces a novel formulation of the Kalman filter that incorporates motion dynamics, allowing the motion model to adaptively adjust according to changes in the object's movement. The proposed Kalman filter substantially improves state estimation, localization, and trajectory prediction compared to the traditional Kalman filter. This is reflected in tracking performance that surpasses recent benchmarks on the KITTI and Waymo Open Datasets, with margins of 0.56% and 0.81% in higher order tracking accuracy (HOTA) and multi-object tracking accuracy (MOTA), respectively. Furthermore, the proposed Kalman filter consistently outperforms the baseline across various detectors. Additionally, it shows an enhanced capability in managing long occlusions compared to the baseline Kalman filter, achieving margins of 1.22% in higher order tracking accuracy (HOTA) and 1.55% in multi-object tracking accuracy (MOTA) on the KITTI dataset. The formulation's efficiency is evident, with an additional processing time of only approximately 0.078 ms per frame, ensuring its applicability in real-time applications.

## 1 Introduction

3D multi-object tracking (MOT) is a vital module for autonomous vehicles (AVs) that provides critical information about their surroundings, allowing them to navigate safely without collision. The MOT methods are either

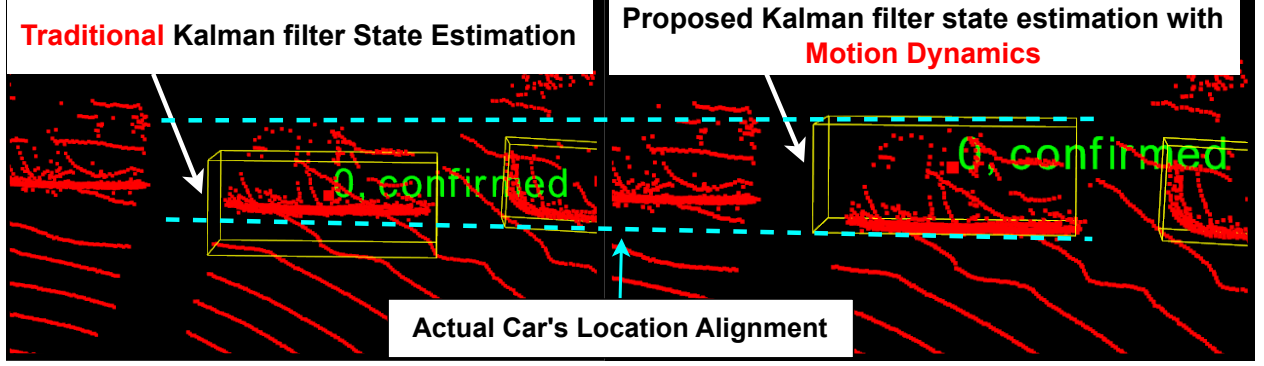


Figure 1: State estimation (**yellow bounding box**) of an off-scene car drifts away from the actual car location (**disconnected lines**) with the traditional Kalman filter. Meanwhile, the proposed Kalman filter with motion dynamics shows robust localization for the car.

algorithm-based (classical) or learning-based approaches; however, classical methods are commonly used due to their substantially lower latency and comparable performance to learning-based approaches. These approaches follow the tracking-by-detection paradigm in which an independent detector is employed to locate objects in a 3D point cloud, followed by a separate tracking algorithm.

Given an object’s current location (measurement), classical methods use Bayesian filters, such as the Kalman Filter (KF), to estimate the object’s next position (state) with uncertainty, a process known as state prediction. The estimation of the object’s state is refined when a new measurement arrives, which is called a state update. In the literature of MOT methods, state prediction estimates the next state of an object based on a constant motion model, such as a constant-velocity or constant-acceleration model. The main limitation of these models is that they do not always reflect the motion status of the objects (motion dynamics). For instance, the state estimation of a car with no change in velocity while employing a constant velocity model has a better state estimation than the constant acceleration or jerk model (3rd derivative of motion equation), as presented in Figure 2 **case A**. On the other hand, when the car accelerates, as shown in Figure 2 **case B**, the constant jerk model has the lowest state estimation error for the car. Similarly, the constant acceleration model outperforms in state estimation when the car exhibits a change in velocity with slight to no change in acceleration, as shown in Figure 2 **case C**.

This behavior has been repeatedly observed in multiple scenarios, indicating that the precision of state estimation from a motion model depends on its alignment with the object’s current motion dynamics. The state estimation precision reduces as the motion dynamics do not match the employed motion model, eventually injecting noise into the state estimation process in the KF that impacts object localization, particularly occluded and off-scene objects, as demonstrated in Figure 1. This work proposes a novel formulation of the KF that accounts for objects’ motion dynamics and adaptively adjusts a dynamic motion model based on observed changes. The proposed solution shows precise state estimation localization (Figure 1) and less trajectory deviation for occluded and off-scene objects over the traditional KF, outperforming recent KITTI and Waymo Open Dataset (WOD) benchmarks.

The contribution of this work can be summarized as follows:

1. Propose a novel formulation for the KF that accounts for object motion dynamics, achieving state-of-the-art performance on KITTI and Waymo Open Dataset (Table 1 and Table 3). The method generalizes the improved tracking performance across various detectors (Figure 7), allowing the recovery of tracked objects for detectors with poor detection performance (Table 2). The proposed KF with motion dynamics significantly enhances state estimation localization for occluded and off-scene objects compared to traditional (baseline) KF (Figure 8). The method improves the estimated trajectories of occluded objects in multiple scenarios (Figure 9).
2. Due to the limited annotations of occluded objects in the current datasets, which prevent sufficient evaluation of MOT methods under challenging conditions, this work introduces a strategy for simulating occlusion scenarios over different occlusion ranges on the public datasets (Section 5.3). The proposed KF with motion dynamics shows substantial performance in prolonged occlusion scenarios, with a margin over the state-of-the-art [1] reaching 1.24 % in HOTA and 1.55% in MOTA, with successful object recovery reaching 1.47% in identification f-score (IDF1), higher than the recent benchmarks (Table 5).

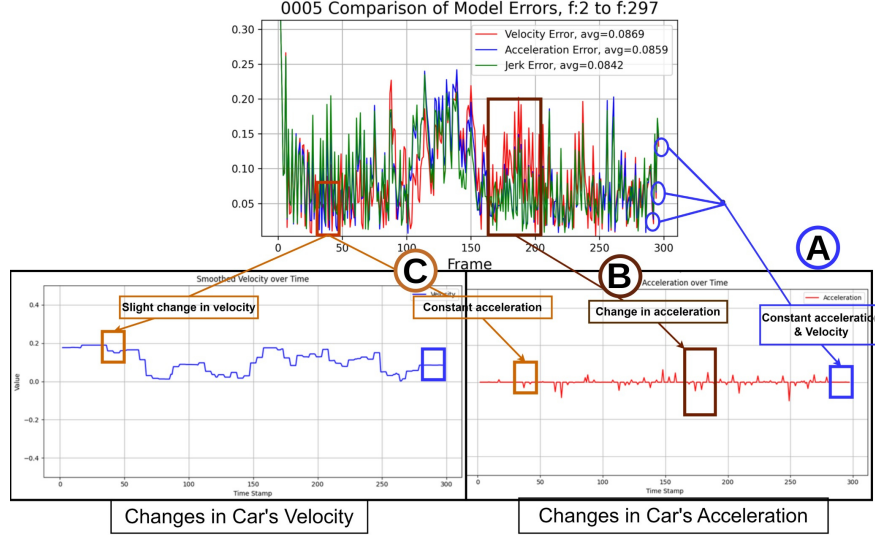


Figure 2: The graph demonstrates the performance fluctuation in state estimation for three motion models: constant velocity (**Red**), constant acceleration (**Blue**), and constant jerk (**Green**). The top graph compares the Euclidean distance error in state estimation obtained by the three models of the 0005 stream in the KITTI [2] dataset. The second row shows graphs of the car’s motion dynamics, change in velocity (**Blue**), and change in acceleration (**Red**).

3. As the opposite of the attempts in the literature, multiple motion models simultaneously, this work maintains the singularity of the assigned motion model that adaptively adjusted as per the captured motion dynamics, resulting in low latency with an average additional computational cost of 0.078 ms per frame (Table 4), making it efficient for real-time applications.

## 2 Related Work

The KF is widely used in MOT literature [3–11], particularly for methods that follow tracking-by-detection paradigms. It predicts the state of tracked objects that nearly resample their actual location and motion states. An imprecise state prediction of an object can lead to failure in the association stage, where the object’s recent position is associated with the closest state prediction. Hence, motion model selection for state prediction in the KF becomes critical in the MOT literature, as it significantly affects tracking performance. The literature shows conflicting preferences for the proper motion model, which has consistently improved state prediction localization. Some methods [7, 8, 10–15] favor the constant velocity model, claiming its outperformance over other motion models. At the same time, other methods [5, 6, 9] utilize the acceleration motion model, as the constant velocity motion model is too simplistic to handle maneuvering in tracking.

For varied reasons, the velocity motion model in the KF is the most commonly used in MOT literature [7, 8, 10–15]. Some MOT methods [7, 10, 13, 14] employ a constant velocity model over others due to its simplicity that facilitates the integration into various frameworks in addition to its lower computational cost, which makes it an efficient choice for real-time systems. Another study [3] has shown that, in some cases, the constant velocity model outperforms higher-degree motion models. Similarly, Na et al. [4] have observed that the constant velocity model is more robust when the target acceleration is slight or unpredictable, especially in noisy environments.

On the other hand, some recent MOT methods [5, 6, 9] adopt a constant acceleration motion model instead of a constant velocity. Part of the recent MOT methods [6, 9] claim that the constant velocity model is trivial and cannot predict precise positions for objects when they face dramatic velocity changes. Wu et al. [6] state that the prediction error accumulates from employing a constant velocity model, which increases exponentially as objects temporarily disappear due to occlusion. In the context of AVs, Reich et al. [9] underline that the maneuvering of a target object depends not only on the target motion but also on the ego motion of the AV. Even though some objects, like parked cars, seem to have no motion, an accelerated AV observes them as objects in motion equal to its motion, which still requires a constant acceleration motion model to handle the ego-motion maneuvering. Despite the maneuvering concerns for objects of MOT methods replacing constant velocity with an acceleration model for state prediction,

Nagy et al. [5] reveal that the tracking performance for occluded objects for MOT methods using constant acceleration can also miss recovering the objects after occlusion due to memory size constraints. The main issue with using a single motion model, either constant velocity or acceleration, is that the performance of state estimation degrades whenever the target’s motion dynamics do not match the assigned motion model, because the current KF formulation neglects motion dynamics.

Further studies [3, 4] show that the motion model’s performance for tracking a target depends on the maneuvers demonstrated by the target. Na et al. [3] conduct experiments that show the constant velocity model is sufficient for non-maneuvering situations, while the constant acceleration model outperforms in maneuvering scenarios. Recent research [4, 16] attempts to tackle this issue by employing an interactive multi-model KF that uses multiple motion models simultaneously, with model selection based on an initial predefined probability for each model. Despite the improvement shown in state estimation, operating multiple motion models simultaneously is highly computationally expensive, particularly in multi-object tracking, where calculations for each model are performed for all targets, in addition to the difficulty of handling sudden motion changes.

Our investigation of the problem shows that the state estimation performance depends on the target’s motion dynamics. Figure 2 shows the state estimation performance of three motion models: velocity, acceleration, and jerk, of a car with many maneuvers. The performance of the jerk model peaks when the car is driving at mixed accelerations. Meanwhile, the acceleration model takes over as the car accelerates consistently. Lastly, the velocity motion model outperforms other models when the car’s velocity is consistent. This scenario shows the importance of considering the target motion dynamics for precise state estimation.

This work addresses the limitation mentioned earlier by proposing a dynamic motion model with a novel formulation of the KF that accounts for the target motion dynamics and adaptively integrates them into the dynamic motion model, eliminating the need to operate multiple motion models while maintaining computational efficiency.

### 3 Methodology

This work addresses the limitations of current motion models and the neglect of object motion dynamics in the standard KF formulation by introducing a novel formulation of the KF state update and state prediction that considers the motion dynamics of objects in state estimation. Figure 3 shows a high-level overview of the pipeline of the proposed formulation of the KF incorporating object motion dynamics. Given an object observed at time  $t - 1$ , the object has three primary parameters: state estimation  $\hat{x}_{t-1|t-1}$  at time  $t - 1$  updated according to a measurement taken at time  $t - 1$ , the state estimation uncertainty covariance  $P_{t-1|t-1}$  at time  $t - 1$ , and weighted motion dynamics  $\hat{w}_{t-1|t-1}$  of the object at time  $t - 1$  updated based on a measurement taken at time  $t - 1$ .

At the prediction step, covered in Section 3.1, the model estimates the next state estimation  $\hat{x}_{t|t-1}$  of the object at time  $t$  of measurement  $t - 1$  through the state-transition model  $F_t$ . As shown in the estimated position state diagram in Figure 3, the state-transition model  $F_t$  maps the state  $\hat{x}_{t-1|t-1}$ , highlighted by red dot-eclipse, to  $\hat{x}_{t|t-1}$ , marked by red eclipse; however, this transition is weighted by the estimated weights of object dynamics  $\hat{w}_{t-1}$  that adjusts the state according to the object motions, marked by blue eclipse. Thus, the obtained  $\hat{x}_{t|t-1}$  is the estimated state at time  $t$  considering the latest dynamics observed at time  $t - 1$ . The state estimation uncertainty covariance will increase as the model becomes uncertain about the new estimate, obtaining an updated covariance  $\hat{P}_{t|t-1}$ .

When a new measurement arrives  $y_t$  at the following time frame  $t$ , the estimated state  $\hat{x}_{t|t-1}$  will be compared and updated according to the new measurement at time  $t$  of the object state to obtain a refined state estimation  $\hat{x}_{t|t}$ . Accordingly, the object dynamics are also updated as per the new measurement, which requires eliminating any noise impact on the measurement localization of the object, as discussed in Section 3.2. The noise mitigation term  $D_t$ , introduced in [1], eliminates the localization noise from the employed detector.

Next, a Gaussian distribution of motion dynamics of the object observed through a time window called the "Smoothing window", discussed in Section 3.4, is formed for each motion dynamic term in the motion model used in the prediction step. In this case, we use a motion model consisting of the position’s first three derivatives (Jerk motion model). Thus, the three Gaussian distribution dynamics shown in the updated motion dynamics graph in Figure 3 represent the change in position (first derivative), change in velocity (second derivative), and change in acceleration



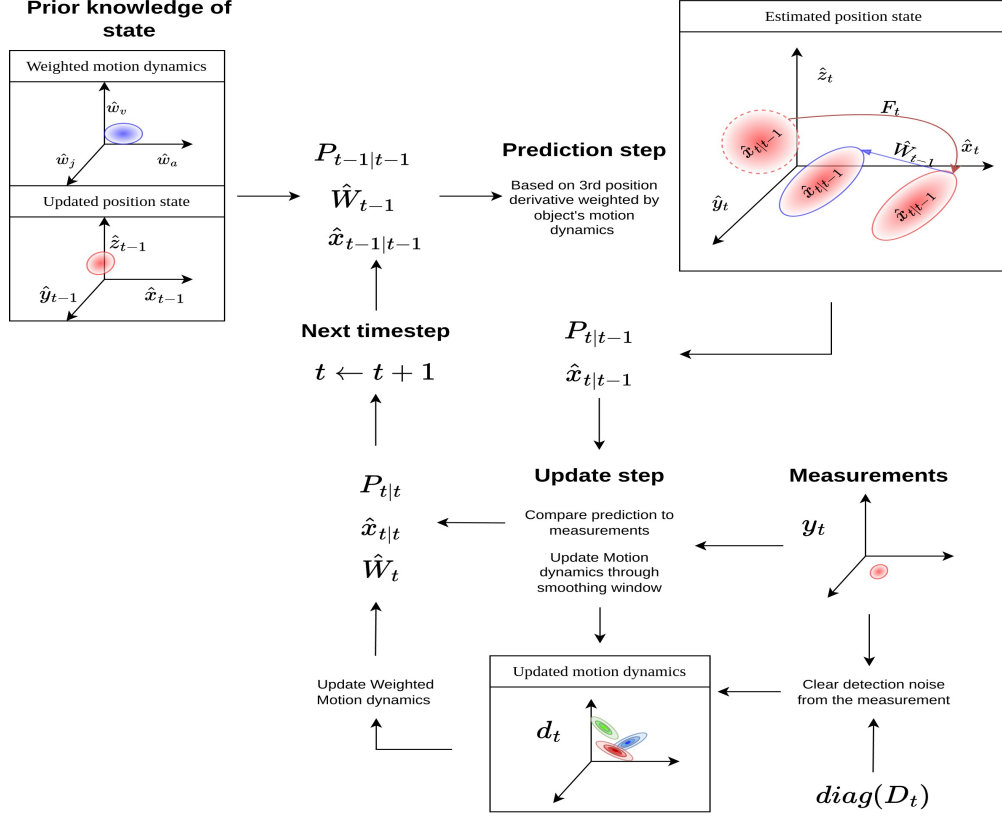


Figure 3: The diagram shows an overview of the proposed Kalman filter incorporating motion dynamics. The flow begins with the prior knowledge of an object's states at time  $t-1$ . The information includes state uncertainty  $P_{t-1|t-1}$ , weighted motion dynamics of the object  $\hat{W}_{t-1}$ , and object's state  $\hat{x}_{t-1|t-1}$ . This information is used to predict the next state estimation of the object, considering its captured motion dynamics, and adjust the estimated state accordingly. This results in the next state estimation  $\hat{x}_{t|t-1}$  and an updated uncertainty  $P_{t|t-1}$ . With a new measurement, the object's spatial state will be updated to obtain  $\hat{x}_{t|t}$ , and new motion dynamics will be captured through the Gaussian distribution of changes observed in motion dynamics parameters (Position, velocity, and acceleration). The obtained updated motion dynamics  $d_t$  from the Gaussian distribution is weighted to form an updated weighted motion dynamics  $\hat{W}_t$ . The flow will be repeated in the next time step  $t+1$ .

(third derivative).

The motion dynamics of the object  $d_t$  at time  $t$  will be adjusted according to the obtained Gaussian distributions of the object's motion dynamics. Then, the weighted motion dynamics  $\hat{w}_t$  will be updated based on the new observed motion dynamics  $d_t$  based on measurement  $y_t$  at time  $t$ . Finally, the state estimation uncertainty covariance  $\hat{P}_{t|t-1}$  decreases as new information about the object's state is observed, in the form of measurement  $y_t$ , to obtain an updated covariance  $\hat{P}_{t|t}$ . Lastly, the procedures will be repeated at each time stamp.

### 3.1 Motion Dynamics in State Prediction

The subsequent estimated state should consider the objects' motion dynamics at the prediction step. In this work, we use the third derivative of the motion equation (Jerk motion equation), which consists of the object's position, velocity, acceleration, and changes in acceleration (Jerk), as shown in Equation 1.

$$x(t) = x_t + v_t t + \frac{1}{2} a_t t^2 + \frac{1}{6} j_t t^3 \quad (1)$$

The main problem of using Equation 1 as a motion model for state prediction in the KF is the assumption of observing the object's motion state velocity  $v_t$ , acceleration  $a_t$ , and jerk  $j_t$  as the absolute motion state of the object. However, this assumption is not valid as the motion state of the object is influenced by the process noise  $P$  and measurement

noise from the update state in the KF. For instance, if a stationary object is observed, its motion state in the KF will still have values for  $v_t$ ,  $a_t$ , and  $j_t$ , leading to a slight deviation of the predicted bounding box. This deviation in prediction accumulates, particularly for occluded objects.

To tackle this issue while maintaining the singularity of the motion model, Equation 1 is weighted by the weighted motion dynamics of the target object  $\hat{w}_t$  as shown in Equation 2.

$$x(t) = x_0 + (\hat{w}_v \cdot v_t)t + \frac{1}{2}(\hat{w}_a \cdot a_t)t^2 + \frac{1}{6}(\hat{w}_j \cdot j_t)t^3 \quad (2)$$

$\hat{w}_v$ ,  $\hat{w}_a$ , and  $\hat{w}_j$  represent the amount of change in the object motion to the motion parameters. For instance,  $\hat{w}_v = \hat{w}_a = \hat{w}_j = 0$  when the observed object is in a stationary state (no motion). In motion, the weight value will change up to the extent of the changes observed in position, velocity, and acceleration, and the motion model will be adjusted to match the object's observed motion dynamics. These motion dynamics can be used to formulate the matrix  $\hat{W}_t$ , representing the target object's recent dynamics at time  $t$ .

$$\hat{W}_t = \begin{bmatrix} 1 & 0 & 0 & 0 \\ 0 & \hat{w}_v & 0 & 0 \\ 0 & 0 & \hat{w}_a & 0 \\ 0 & 0 & 0 & \hat{w}_j \end{bmatrix} \quad (3)$$

Accordingly, the next state prediction of the KF can be presented as follows:

$$\hat{\mathbf{x}}_{t|t-1} = \mathbf{F}_t \hat{\mathbf{W}}_{t-1} \hat{\mathbf{x}}_{t-1|t-1} \quad (4)$$

Where  $F_t \hat{W}_{t-1}$  maps the current state  $\hat{x}_{t-1|t-1}$  to the next state  $\hat{x}_{t|t-1}$  based on measurement  $t - 1$  by considering the objects motion dynamics observed at time  $t - 1$ .

### 3.2 Localization Term Selection for Motion Dynamics

Acquiring data that perceives the motion dynamics of objects is a critical part of this work. Neglecting the motion dynamics can lead to dramatic drift in the estimated state of the objects. The motion dynamics of an object can be perceived across consecutive measurements of its states. As shown in Equation 5, acquiring and perceiving the amount of change in position and velocity requires at least three successive position states of the object, assuming  $z$  is the object's actual position.

$$\begin{aligned} \text{Velocity: } \Delta z_t &= z_t - z_{t-1}, \\ \sigma_{\Delta z_t} &\propto \text{acceleration fluctuations,} \\ \text{Acceleration: } \Delta^2 z_t &= \Delta z_t - \Delta z_{t-1}, \\ \sigma_{\Delta^2 z_t} &\propto \text{jerk fluctuations.} \end{aligned} \quad (5)$$

Equation 5 computes the amount of change required to provide an estimation of the motion dynamics for the jerk motion model, as discussed in Section 3.3; however, an accurate measurement of the objects' position  $z_t$  is needed to obtain it. Since the actual position of the objects is unavailable,  $z_t$  can be replaced by three potential terms representing the objects' position state. The first option is the **measurement** from the employed detector,  $\mathbf{z}_t$ , at time  $t$ . The second option is the **updated state estimation**  $\mathbf{x}_{t|t}$  of measurement  $t$  at time  $t$ . The third option is to use detection measurement  $\mathbf{z}_t$  (from the first option) and use the noise mitigation detection  $\mathbf{D}_t$  proposed in [1] to remove any noise coming from the detector (**Post measurement**).

To determine which term better represents the objects' actual location, an experiment is conducted on the KITTI [2] dataset across multiple streams, evaluating the localization performance of each term to the objects' actual locations from the ground truth. At each timestamp, each term is computed for all objects, and the localization error is calculated using Euclidean distance to the actual location of these objects.

Figure 4 shows a graphical representation of the Euclidean distance error between the localization obtained from each term discussed earlier and the actual localization of two cars from the ground truth localization. The post-measurement term shows the closest capture of the car's localization to the ground truth, achieving the lowest mean square error and standard deviation, which matches the observations in work [1].

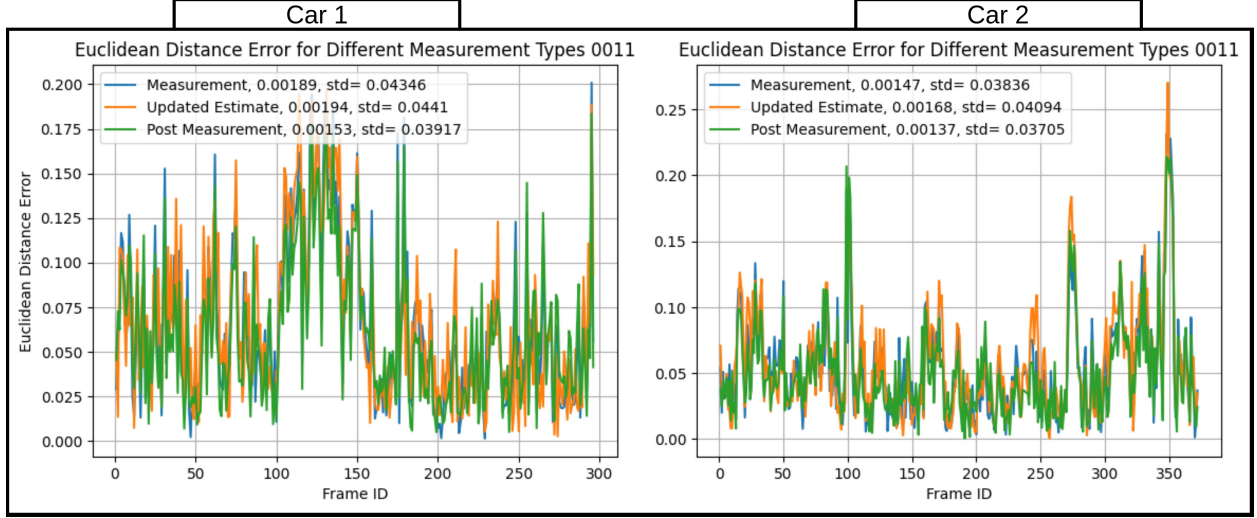


Figure 4: The graph shows the Euclidean distance error comparison between the localization measurements obtained from the employed detector (**Blue-line**), the updated state estimation of the object's location (**Orange-line**), and the measurement from the detector with cleared noise by the proposed term  $D_t$  (**Green-line**). The experiment is conducted in two cars over more than 300 consecutive frames. The numerical values in the legend present the mean square error and standard deviation, respectively.

To this end, the post-measurement (third) term is used to determine the recent position of objects. The term is computed by eliminating the localization noise from the detector  $D_t$ , as presented in [1], from the measurement  $z_t$  and obtaining the post-measurement localization  $\hat{z}_t$ .

$$\hat{z}_t = z_t - (HK_t) \text{diag}(D_t) \quad (6)$$

As shown in Equation 6, Kalman gain  $K_t$  is incorporated into the noise residual,  $\text{diag}(D_t)$ , to include the model uncertainty while clearing the noise from the measurement. Since  $K_t$  is in the estimation space,  $H$  maps it to the measurement space. Finally, the obtained refinement noise is removed from the measurement.

### 3.3 Temporal Evolution in Motion Dynamics Estimation

As shown in Equation 5, three consecutive observations of an object's position are used to quantify the fluctuation in an object's velocity and acceleration motion dynamics. Nevertheless, a single quantification is insufficient to conclude an object's motion dynamics since external noise could impact the measurement  $z_t$ . A distribution of multiple quantifications can provide a more accurate estimation of an object's motion dynamics. The distribution of consecutive quantifications of motion dynamics parameters (position  $z_t$ , velocity  $\Delta z_t$ , and acceleration  $\Delta^2 z_t$ ) of an object, obtained from Equation 5, resamples a 2D Gaussian distributions in x and y directions, as shown in Figure 3 (*Updated motion dynamics*). The distribution of each motion dynamics parameter shapes a Gaussian distribution around its potential value.

To obtain an estimation of an object's motion dynamics, consider a single motion parameter: fluctuation in velocity  $\sigma_{\Delta z_t}$ . Assume a car drives at a constant velocity. The amount of change in position (traveling distance) value  $\Delta z_{t \leftarrow s}$  from time  $s$  to time  $t$  will remain constant, which refers to the mean of the distribution  $\Delta \bar{z}$ . In this case, the deviation of the data  $\sigma_{\Delta z_{t \leftarrow s}}$  from the mean will be approximately zero. On the other hand, if the car starts to drive at a variable velocity, the amount of change in position will change over time. In this case, the deviation of the data from the mean increases as the variation in velocity increases. Thus, the standard deviation  $\sigma_{\Delta z_{t \leftarrow s}}$  approximates the fluctuation in the velocity motion dynamics of the object from time  $s$  to time  $t$ . Given the consecutive readings and the gradual behavior of objects' motion, the formulation will shape a Gaussian distribution.

In other words, the standard deviation  $\sigma_{\Delta z_{t \leftarrow s}}$  increases when the car accelerates, resulting in varying travel distance changes over time. This increased variance in traveling distance widens the Gaussian distribution, thereby enlarging  $\sigma_{\Delta z_{t \leftarrow s}}$ . Hence,  $\sigma_{\Delta z_{t \leftarrow s}}$  reflects not only changes in velocity but also quantifies fluctuations in acceleration. Gen-

eralizing this relationship to motion dynamics parameters (velocity  $\Delta z$ , acceleration  $\Delta^2 z$ ), the motion dynamics for observations from time  $s$  to  $t$  (with  $k = t - s + 1$  total observations) are estimated as:

$$\sigma(\Delta\theta_{t \leftarrow s}) = \sqrt{\frac{1}{k-1} \sum_{i=1}^k (\Delta\theta_i - \overline{\Delta\theta})^2},$$

where  $\Delta\theta \in \{\Delta z, \Delta^2 z\}$ ,

$$\overline{\Delta\theta} = \frac{1}{k} \sum_{i=1}^k \Delta\theta_i.$$
(7)

Here,  $\Delta\theta_{t \leftarrow s}$  represents the finite differences of velocity ( $\Delta z$ ) or acceleration ( $\Delta^2 z$ ) over the time window  $t \leftarrow s$ , and  $\overline{\Delta\theta}$  denotes their sample mean. The standard deviation  $\sigma(\Delta\theta_{t \leftarrow s})$  quantifies fluctuations in the corresponding motion parameter.

The motion dynamics estimation vector  $d_t$  is then derived as:

$$d_t = \begin{bmatrix} 1 \\ \sigma(z_{t \leftarrow s}) \\ \sigma(\Delta z_{t \leftarrow s}) \\ \sigma(\Delta^2 z_{t \leftarrow s}) \end{bmatrix},$$

where

(8)

$\sigma(z_{t \leftarrow s})$  captures **position fluctuations**,  
 $\sigma(\Delta z_{t \leftarrow s})$  corresponds to **velocity fluctuations**,  
 $\sigma(\Delta^2 z_{t \leftarrow s})$  reflects **acceleration fluctuations**.

### 3.4 Motion Dynamics Transition and Smoothing Window

As demonstrated in Equation 7, the estimation of motion dynamics can be obtained from the distribution of  $\sigma(\Delta\theta_{t \leftarrow s})$  across  $k$  consecutive measurements. The determination of  $k$ , called transition window size, should be carefully selected as it controls when the model alternates from one motion dynamic state to another.

For a better understanding of the motion dynamic transition and its influence on the state estimation, Figure 5 shows a use case of a car that accelerates and then decelerates. The car starts to **accelerate** at **frame 140 to 160**, as shown in the second graph when the change in distance shifts. The error in state estimation of the constant acceleration and jerk models decreases as expected, while increasing for the constant velocity model. From **frame 160 to 168**, there is a **transition** in the motion dynamics as the car starts to decelerate. At the transition state, the constant velocity yields the lowest error as the change in velocity approaches 0. This transition state is essential to consider while selecting the size of the transition window  $k$ . The large window size can cause the failure to capture changes in motion dynamics that occur quickly, as shown in the transition state of Figure 5. On the other hand, a window that is too small can cause quick motion state transitions, which also impact the stability of the estimated state.

The transition window size  $k$  determines how many observations are needed to gather adequate information about the object's motion dynamics. The window size controls the motion dynamics weights, as presented in Equation 3, which adjusts the state estimation based on the observed motion dynamics. Figure 6 shows how different transition window sizes impact the motion dynamics weights presented in Equation 3.

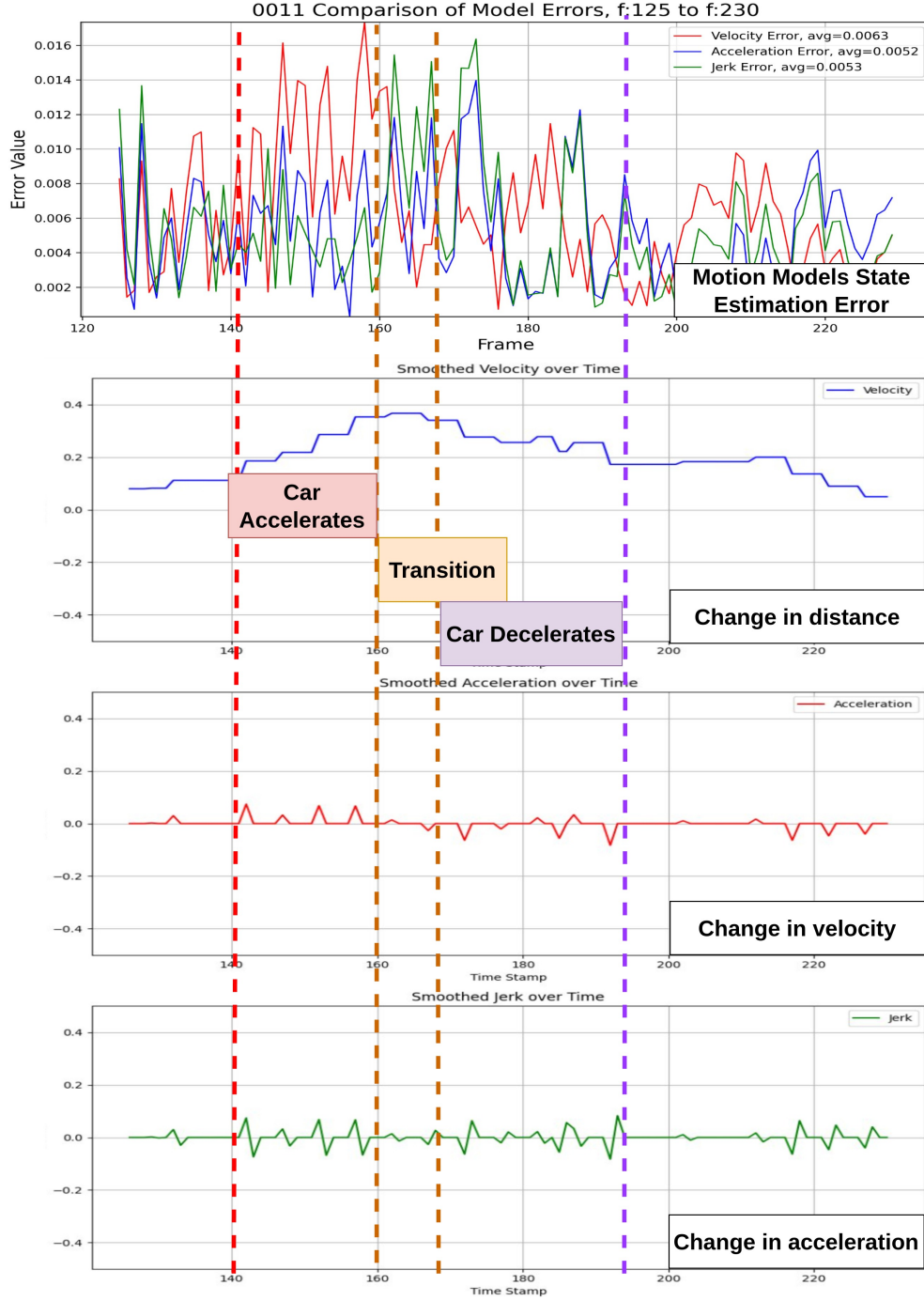


Figure 5: The graphs show a car's motion dynamics, which accelerates and decelerates for a particular time stamp. The first graph shows the Euclidean distance error of state estimation from three different motion models: constant velocity (**Red**), constant acceleration (**Blue**), and constant Jerk (**Green**). The second graph shows the corresponding change in traveling distances from the ground truth, presenting the car motion dynamics for velocity. Meanwhile, the third graph shows the car's velocity change compared to the ground truth, illustrating the motion dynamics for acceleration. The last graph shows the change in car acceleration from the ground truth, illustrating the motion dynamics for jerk. The graph highlights three transition states in the motion dynamics of the car: Acceleration (**Red dot-line**), transition from acceleration to deceleration (**Orange dot-line**), and deceleration (**Violet dot-line**).

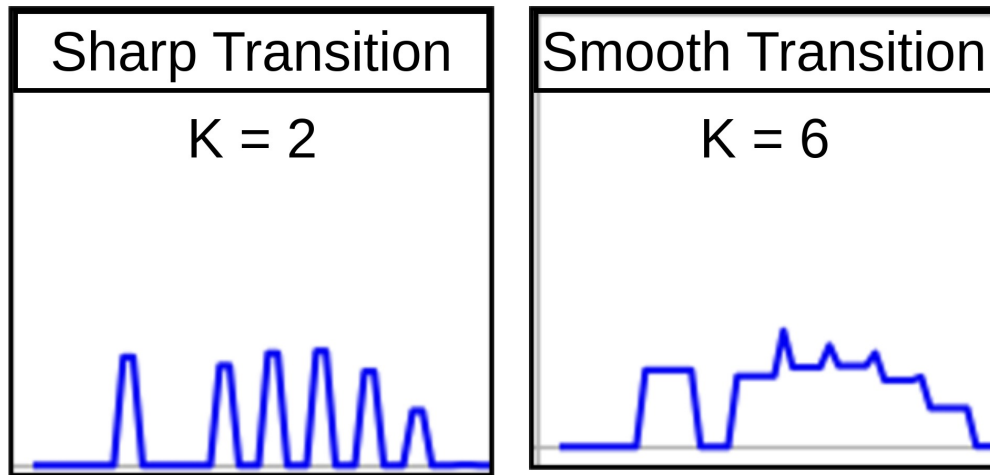


Figure 6: The graphs show the impact of the smoothing window of sizes 2 and 6 on the motion dynamics weight that responds to transitions between motion models. With a small smoothing window, the transition between models becomes sharp, causing an immediate switch; on the other hand, a larger window size shows smoother transitions.

## 4 Weighted Motion Dynamics Evolution for State Update

The obtained motion dynamics vector  $d_t$  cannot be used directly as weights into the motion parameters in Equation 2 because the standard deviation values can be between  $[0, \infty]$ , they must be normalized to be in the range  $[0, 1]$ . For instance, constant velocity motion model can be obtained from Equation 2 when  $\hat{w}_a = \hat{w}_j = 0$ . Meanwhile, the constant acceleration model can be obtained when  $\hat{w}_j = 0$ . Hence, the primary purpose of the weights is to alternate between the three derivative models. Thus, the amount of change the model needs to alternate from one motion model to another must be determined, which will be used to normalize  $d_t$ . This amount of change is called the motion dynamics factor donated by  $\ell_t$ , which should be fine-tuned for all three derivatives. Assuming a one-dimensional space, the motion dynamic factor will be:

$$\ell_t = [1 \quad \ell_v \quad \ell_a \quad \ell_j]$$

Accordingly, the weighted motion dynamics are obtained as:

$$\begin{aligned} \hat{w}_v &= \min \left( \frac{\sigma(z_{t \rightarrow k})}{\ell_v}, 1 \right), \\ \hat{w}_a &= \min \left( \frac{\sigma(\Delta z_{t \rightarrow k})}{\ell_a}, 1 \right), \\ \hat{w}_j &= \min \left( \frac{\sigma(\Delta^2 z_{t \rightarrow k})}{\ell_j}, 1 \right). \end{aligned} \quad (9)$$

The normalization procedure can be formalized algebraically as matrix operations, as shown in Equation 10.

$$\begin{aligned} d_{t_{\text{norm}}} &= d_t \circ \ell_t^{-1}, \\ \hat{w}_t &= \frac{1}{2} (\mathbf{1}_n + d_{t_{\text{norm}}} - |\mathbf{1}_n - d_{t_{\text{norm}}}|). \end{aligned} \quad (10)$$

By Equation 10, the weights are updated by the current evolution in the motion dynamics of objects.

## 5 Results and Discussion

This work proposes a formulation of the KF that accounts for the motion dynamics of tracked objects. For adequate evaluation of the proposed formulation, the tracking framework proposed in the state-of-the-art work [1] is used, and the traditional KF is replaced with the proposed KF formulation in this work. The evaluation procedures consist of quantitative evaluation, qualitative evaluation, run-time performance, and an ablation study about challenging scenarios in tracking. The quantitative (Section 5.2.1) and qualitative assessments (Section 5.2.2) show the tracking performance and enhanced localization of state estimation compared to recent benchmarks on KITTI [2] and the WOD [17]. The performance evaluation is extended in Section 5.2.3 to include a run-time comparison of the traditional KF and the proposed KF, quantifying the difference in computational cost. Lastly, an ablation study is conducted, Section 5.3, to evaluate the tracking performance of simulated occlusion scenarios that assesses the proposed KF with motion dynamics performance of tracking occluded objects compared to the traditional KF.

### 5.1 Environment Setup

This experiment uses an AMD Ryzen 6900HX processor with 32 GB of RAM (Single CPU); no GPU is involved. The KF formulation is implemented from scratch using the Eigen3 library in C++17. Additionally, OpenCV 4.6 and PCL 1.14 libraries are used for visualization. All performance evaluations in this work are done using the official evaluation tools from KITTI [2] and WOD [17].

### 5.2 Comparison with Benchmarks

#### 5.2.1 Quantitative Evaluation

This section consists of three parts of this work's quantitative evaluation of the proposed KF. The first **Part (B.I)** evaluates the overall tracking performance of the proposed KF embedded in RobMOT [1] work with recent benchmarks, including RobMOT [1] with a baseline KF. Next, the performance generalization of the proposed work is discussed in **Part (B.II)**, which assesses its performance using various detectors compared to the baseline KF. Lastly, the tracking performance in challenging conditions, such as tracking distant targets, is evaluated in **Part (B.III)** to quantify the



performance difference between the proposed KF with motion dynamics and the baseline KF used in the literature.

**(I) Evaluation with State-of-the-art Methods:** The initial evaluation uses the benchmarks from the KITTI leaderboard [2] on the test dataset. Table 1 contains the RobMOT work [1] with the baseline KF donated by *RobMOT (Baseline)* and the integrated version with the motion dynamics proposed in this work donated by *RobMOT (Dynamic)*. Although the annotated occlusion scenarios in the KITTI dataset are limited, which makes the evaluation of this work challenging, similar to the WOD, the proposed KF with motion dynamics outperforms the recent state-of-the-art RobMOT and the baseline KF and other benchmarks. However, the improvement is slight as the proposed KF with motion dynamics concerns localization for state estimation of objects, which requires occlusion scenarios to demonstrate its significance, as shown in Sections 5.2.2 and 5.3.

Table 1: Comparison with the recent state-of-the-art MOT methods on the KITTI test dataset

Method	HOTA	MOTA	AssA	AssRe	IDSW
TripletTrack [18]	73.58%	84.32%	74.66%	77.3%	322
PolarMOT [19]	75.2%	85.1%	76.95%	80.0%	462
DeepFusion-MOT [20]	75.5%	84.6%	80.1%	82.6%	84
Mono-3D-KF [9]	75.5%	88.5%	77.6%	80.2%	162
PC3T [21]	77.8%	88.8%	81.6%	84.8%	225
MSA-MOT [7]	78.5%	88.0%	82.6%	85.2%	91
UG3DMOT* [8]	78.6%	87.98%	82.28%	85.36%	30
CasTrack* [6]	77.3%	86.29%	80.29%	83.12%	184
VirConvTrack+ [6,22]	79.9%	89.1%	82.6%	85.6%	201
RobMOT* [1] (Baseline)	81.22%	90.48%	85.77%	89.68%	<b>6</b>
RobMOT* (Dynamic)	<b>81.29%</b>	<b>90.55%</b>	<b>85.85%</b>	<b>89.72%</b>	<b>6</b>

**(II) Performance Generalization Evaluation Across Various Detectors:** Another experiment has been conducted to evaluate the generalization of the improvement for the proposed KF (Dynamic) across five detectors, comparing it with the baseline KF in the literature. The following experiments are done by replacing the traditional KF in RobMOT (Baseline) [1] with the proposed KF for motion dynamics (Dynamic) in this work.

The first experiment is conducted on the KITTI validation dataset using two different motion models: acceleration and jerk motion models. In Figure 7, the traditional KF is marked as the baseline, and the proposed KF is marked as dynamic. In the case of the acceleration model, the proposed KF with motion dynamics will alternate between velocity and acceleration based on the estimated motion dynamics. Similarly, the proposed KF will alternate between velocity, acceleration, and jerk in the case of the Jerk motion model. Figure 7 shows the tracking performance of state estimation obtained from the baseline KF and the proposed KF on HOTA and MOTA metrics.

As shown in Figure 7, the proposed KF consistently outperforms the baseline across the five detectors in HOTA and MOTA. The improvement reaches 0.50% in MOTA and 0.24 in HOTA with the PvCNN [23] detector using the Jerk motion model. This result indicates the generalization of the improvement in tracking by employing the proposed methodology. Furthermore, the proposed KF (Dynamic) reduces the identity switch (IDSW) in PointRCNN [24] and Second [25], as demonstrated in Table 2. This result indicates that the enhancement in state estimation from the proposed KF leads to recovering objects under occlusion or conditions that disturb their visibility to the detector.

**(III) Tracking Performance Evaluation for Distant Targets:** A similar experiment setup is conducted on the WOD using CasA [27] and CTRL [28] detectors; however, this experiment divides the tracking performance across three distance ranges: 0 to 30 meters (Close targets), 30 to 50 meters (Moderate distanced targets), and 50 to +inf meters (Distant targets). Table 3 presents the improvement obtained by replacing the baseline KF with the proposed KF in this work. The table shows the performance for acceleration and jerk motion models at two different levels, indicating the difficulty of the tracking condition: Level 1 (Easy-Moderate) and Level 2 (Moderate-Hard). The proposed KF consistently improves MOTA and reduces object mismatching (Miss) in both motion models. Moreover, the improvement increases as targets become distant from the observer (AV), as shown in Table 3 (Range [50, +inf]). The enhancement in performance reaches close to 1% in MOTA, and there is a similar reduction in Miss for targets in distances of more than 50 meters (Distant targets).

The experiment underscores the importance of considering motion dynamics in the KF for distant objects, as their motion becomes distorted and requires a more complex motion model for state estimation.

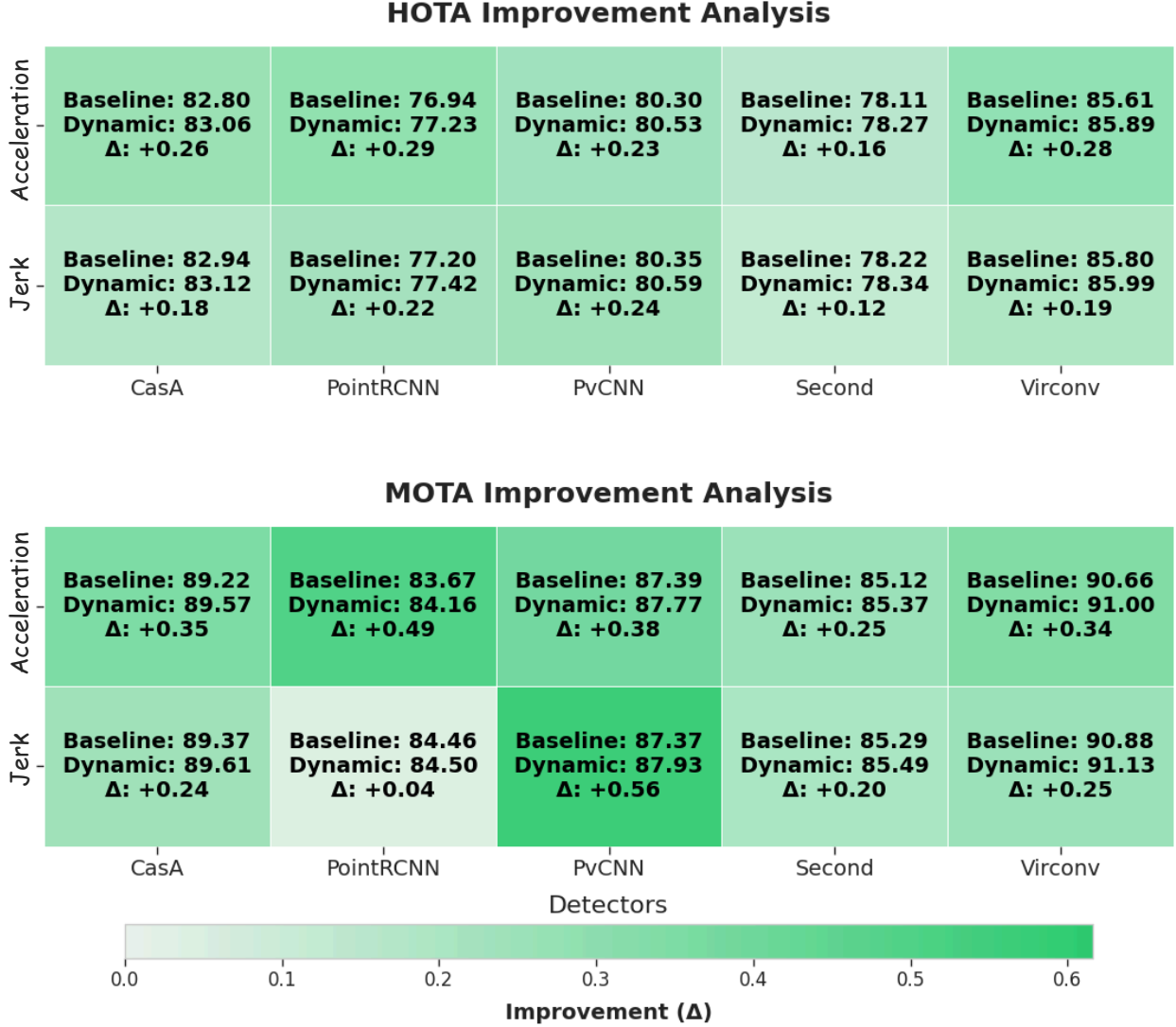


Figure 7: A comparison with the state-of-the-art RobMOT [1] with the baseline Kalman filter and the proposed Kalman filter with motion dynamics on the KITTI validation dataset across five detectors.

In summary, the proposed KF with motion dynamics consistently outperforms the traditional KF in KITTI and WOD in recent benchmarks (Table 1, Figure 7, and Table 3). The improvement is generalized across various detectors (Figure 7), with a reduction in identity switches (Table 2) for objects that face challenging tracking conditions, such as occlusion, which prevents object mismatching. The results align with those obtained from the WOD (Table 3), where the improvement remains consistent across two detectors, with a reduction in mismatched objects. Furthermore, the improvement in tracking increases significantly as the targets become distant from the AV, showing the need to consider motion dynamics, a more complex motion model, for state estimation.

### 5.2.2 Qualitative Evaluation

This section discusses the performance of state estimation, localization, and trajectory estimation for the proposed KF with motion dynamics compared to the baseline KF in the literature. The first part of this section, **Part (I)**, evaluates the localization performance of the state estimation in two challenging tracking scenarios: occlusion and off-scene targets. In the second part, **Part (II)**, a trajectory estimation evaluation is conducted for two occluded objects to assess

Table 2: Identity switch performance comparison with the state-of-the-art RobMOT [1] with the baseline Kalman filter and the proposed Kalman filter with motion dynamics on the KITTI validation dataset across five detectors.

Motion Model	Virconv [26]	CasA [27]	PointRCNN [24]	PvCNN [23]	Second [25]
<b>Baseline (RobMOT)</b>					
Acceleration	1	1	5	1	1
Jerk	1	1	6	1	3
<b>Dynamic (RobMOT-Dynamic)</b>					
Acceleration	1	1	4	1	1
Jerk	1	1	4	1	1
<b>Improvement (Reduction)</b>					
Acceleration	0	0	+1	0	0
Jerk	0	0	+2	0	+2

**Color Key:** Significant reduction in IDSW

**Note:** Positive values indicate a reduction in identity switches. Values represent absolute counts.

Table 3: Performance Improvements obtained from the proposed Kalman filter with motion dynamics over RobMOT [1] with baseline Kalman filter with Level 1 &amp; Level 2 (CasA [27] &amp; Ctrl Detectors [28]) on WOD

Detector	Range (m)	Acceleration				Jerk			
		Level 1		Level 2		Level 1		Level 2	
		MOTA↑	Miss↓	MOTA↑	Miss↓	MOTA↑	Miss↓	MOTA↑	Miss↓
CasA	[0, 30)	+0.25%	-0.35%	+0.26%	-0.35%	+0.44%	-0.56%	+0.45%	-0.13%
CasA	[30, 50)	+0.46%	-0.62%	+0.47%	-0.25%	+0.81%	-0.40%	+0.81%	-0.80%
CasA	[50, +inf)	+0.56%	-0.27%	+0.53%	-0.83%	+0.85%	-1.09%	+0.78%	-0.95%
Ctrl	[0, 30)	+0.09%	-0.05%	+0.09%	-0.08%	+0.25%	-0.12%	+0.25%	-0.13%
Ctrl	[30, 50)	+0.27%	-0.33%	+0.29%	-0.14%	+0.63%	-0.49%	+0.63%	-0.31%
Ctrl	[50, +inf)	+0.38%	-0.17%	+0.36%	-0.17%	+0.56%	-0.66%	+0.53%	-0.95%

**Color Key:**

Small: MOTA ↑ < +0.3%, Miss ↓ > -0.3%  
Moderate: MOTA ↑ +0.3 to 0.6%, Miss ↓ -0.3 to 0.6%  
Large: MOTA ↑ > +0.6%, Miss ↓ < -0.6%

the formed trajectory from estimated states for the targets during the occlusion using baseline and proposed KF.

**(I) State Estimation Localization Evaluation in Occlusion and Off-scene Scenarios:** This experiment assesses the localization precision of state estimation for occluded and unobservable targets from the proposed KF with motion dynamics compared to the baseline KF. Figure 8 shows two scenarios: The first involves two parked cars occluded by a van, and the second involves three cars leaving the field of view of the LiDAR sensor (Off-scene). The actual location of the cars during occlusion is highlighted by a disconnected purple 2D box, as shown at the top left in Figure 8. The comparison is done on acceleration and jerk motion models, where the right side of Figure 8 shows the performance in the two scenarios using the acceleration motion model, and the left side shows the performance using the jerk motion model. The comparison uses RobMOT [1] with a baseline KF and the proposed KF with motion dynamics.

In the first scenario, two cars with IDs 1 (*Car: ID1*) and 5 (*Car: ID5*) are occluded by a van. The last state estimation of *Car: ID1* before the occlusion ends is marked by (Sc1: (A) **Car ID:1**) and (Sc1: (B) **Car ID:5**) for *Car: ID5* in the second row in Figure 8. Both cars are occluded for about 10 frames. As shown in (Sc1: (A) **Car ID 1**) in Figure 8, the proposed KF with motion dynamics shows a precise localization of *Car: ID1* compared to the baseline KF. A similar performance is observed for *Car: ID5* in (Sc1: (B) **Car ID5**), where the estimation from the baseline KF completely drifts from the car’s actual location while the proposed KF estimation overlaps. The performance is consistent in both the acceleration and jerk motion models, which shows the adaptation of the proposed KF with the observed dynamics regardless of the employed motion model.

On the other hand, the second scenario involves three cars, *Car: ID0*, *Car: ID1*, and *Car: ID2*, which leave the lidar sensor’s field of view, making it an off-scene scenario. The last state estimation of *Car: ID1* is marked by (Sc2: (A) **Car ID:1**), while *Car: ID0* and *Car: ID2* are marked by (Sc2: (B) **Car ID:0**) and (Sc2: (C) **Car ID:2**) in Figure 8, respectively. Although the state estimation of *Car: ID1* and *Car: ID2* from the baseline KF shows a pretty good

overlap with the actual location of the cars, with a slight shift to the left in *Car:ID1* and to the bottom in *Car:ID2*, this slight shift in their state estimation almost disappears when the proposed KF with motion dynamics is employed. The proposed KF shows accurate state estimation localization for *Car:ID1* and *Car:ID2* compared to the baseline KF. This outcome can be easily observed in (Sc2: (B) Car ID:0), where the state estimation of the baseline KF significantly shifted from the actual car location; meanwhile, the state estimation from the proposed KF with motion dynamics precisely localizes *Car:ID0*. This result shows the localization precision of the proposed KF compared to the baseline KF used in the literature.

**(II) Trajectory Estimation Evaluation for Occluded Targets** This experiment evaluates the state estimation trajectory obtained from the baseline KF and the proposed KF with motion dynamics for an occluded target. The evaluation is done on two motion models: acceleration and jerk motion models. The area surrounded by a red disconnected bounding box in Figure 9 shows state estimations during the occlusion period. The top graph shows the occlusion scenario using the acceleration motion model. In contrast, the bottom figure uses the jerk motion model. Tables inside each graph contain the localization error for state estimations obtained from the baseline KF (Constant Acceleration/Jerk) and the proposed KF with motion dynamics (Dynamic Model) to the car's actual location from the ground truth. The nearest state estimation to the ground truth from both models is connected to the ground truth line by a disconnected line from each state colored by the same color as the model that obtained the nearest estimation, orange for the baseline, and blue for the proposed KF.

Figure 9 shows that most state estimations from the proposed KF are the nearest to the ground truth, connected by a disconnected line, in both acceleration and jerk motion models. The results are also highlighted in the error tables in the graphs, which show a lower distance error for state estimations from the proposed KF compared to the baseline. This experiment shows the consistent outperformance of the proposed KF in state estimation precision compared to the baseline during occlusion.

In summary, experiments (B.2.I) and (B.2.II) show that the proposed KF outperforms the baseline used in the literature in state estimation, localization, and trajectory formation during occlusion and off-scene scenarios. In (B.2.I), the

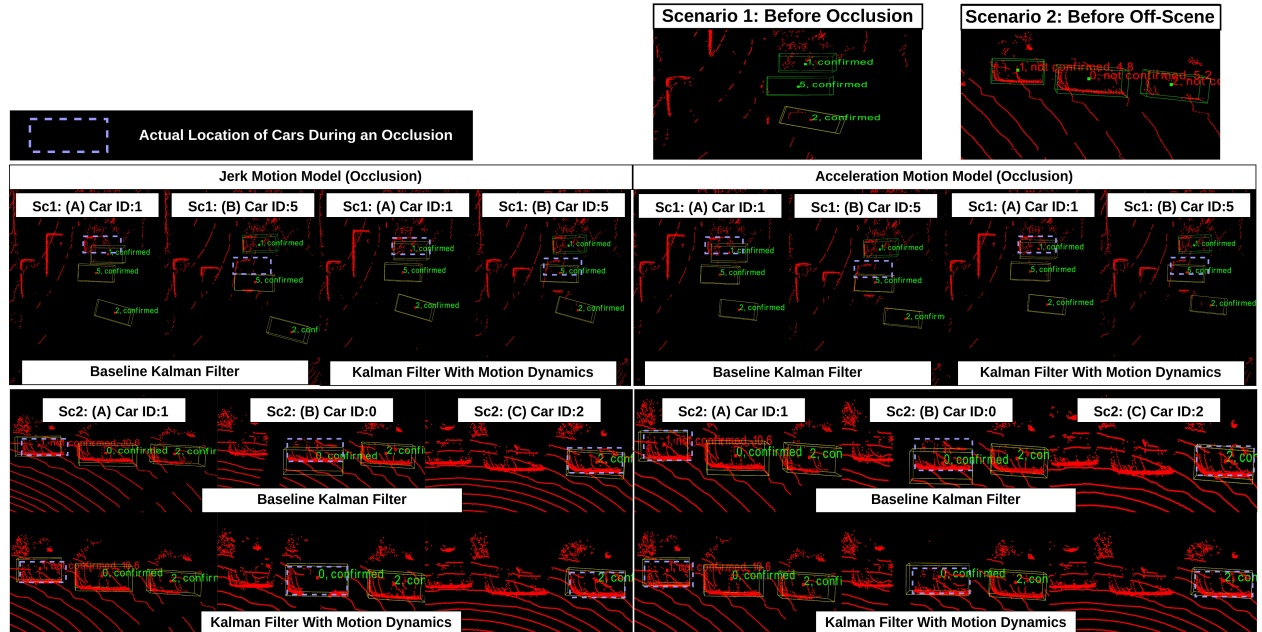


Figure 8: The figure shows two challenging scenarios of object tracking. The first scenario (Sc1) presents two cars occluded by a van. The second scenario (Sc2) shows three cars leaving the scene (off-scene). The letters A, B, and C present an occlusion of a specific object. State estimation obtained from the baseline and proposed KF, integrated in RobMOT [1], is presented as a **3D yellow bounding box** in the scenes. The left side shows the performance by employing the jerk motion model. In contrast, the right side shows the performance using the acceleration motion model.

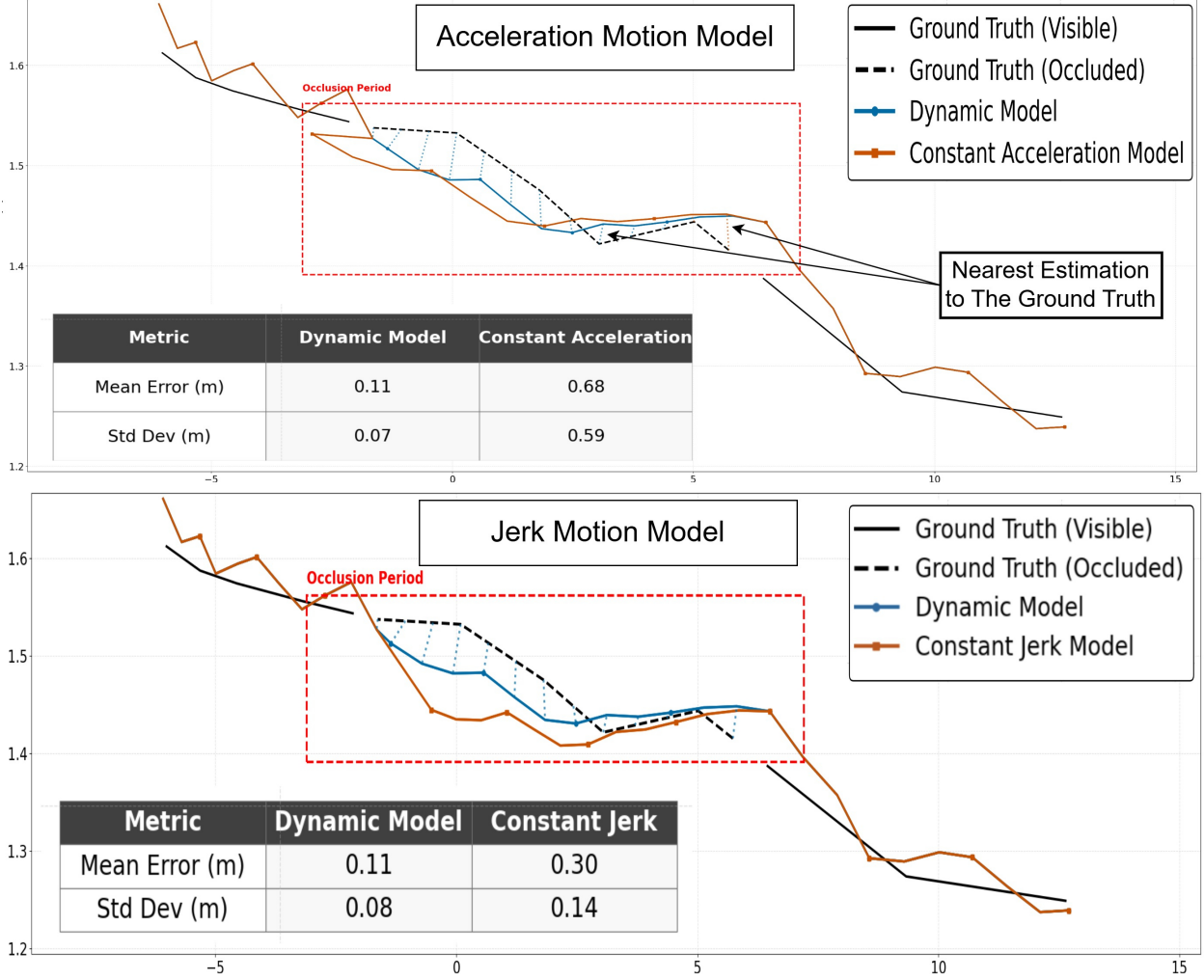


Figure 9: State estimation trajectory comparison of an occluded car between the proposed Kalman filter with motion dynamics and the baseline Kalman filter. The nearest states to the car’s original location during the occlusion are marked disconnected lines from the state to the ground truth, colored by the same color as the model obtained for the state. The tables present the mean and standard deviation of the state estimation for each model relative to the ground truth.

proposed KF with motion dynamics maintains precise localization for the cars in Figure 8 regardless of the employed motion models, which shows the advantage of integrating motion dynamics into state estimation. Furthermore, the proposed KF shows consistent close state estimations to the actual location of the target object during the occlusion, forming a more accurate trajectory to the object movement than the baseline KF, as shown in Figure 9 in (B.2.II).

### 5.2.3 Run-time Performance Comparison

This section discusses run-time performance experiments to approximate the cost of including motion dynamics in the KF. The experiments involve five detectors on the combined training and validation KITTI dataset. RobMOT [1] is run by employing the baseline KF and the proposed KF with motion dynamics, and the frame per second (FPS) is recorded for each across the five detectors. Next, the time per frame in milliseconds is obtained from the collected FPS for each detector presented in Table 4. The difference in the running time between the baseline and the proposed KF is computed as shown in the last row in Table 4 under the heading (Additional Time). Table 4 demonstrates that the processing cost of the proposed KF with motion dynamics increases the computational time per frame by 0.078 ms on average. This result indicates that employing the proposed KF does not impact the run-time efficiency of the system (tracking methods), making it suitable for real-time applications.

Table 4: Processing time per frame comparison between the proposed and baseline Kalman filter across five detectors on the KITTI dataset

Metric	Virconv	CasA	PointRCNN	Second	PvCNN
Baseline Time (ms)	0.542	0.585	0.859	0.643	0.613
Dynamic Time (ms)	0.615	0.653	0.953	0.714	0.696
<b>Additional Time (ms)</b>	<b>0.073</b>	<b>0.068</b>	<b>0.094</b>	<b>0.071</b>	<b>0.083</b>

### 5.3 Ablation Study

Occlusion scenarios in KITTI and WOD are limited, which limits the evaluation of tracking methods on challenging tracking conditions. Thus, this work introduces a strategy for evaluating MOT methods on occlusion scenarios by simulating them from original datasets and using detectors. In this study, we generate simulated occlusion cases where detections for some targets have been detached from the original detections input to the tracker. This occurs when an object is occluded, losing observation of it for a specific period. The experiment setup is explained in Section 5.3.1, and the evaluation of the simulated occlusion scenarios is discussed in Section 5.3.2.

#### 5.3.1 Simulated Occlusion Scenarios

The occlusion of an object consists of successive frames with no observation of the object and no detections from the detector. Hence, eliminating some consecutive detections for a particular object simulates the occlusion phenomenon; however, the elimination should not be random. Since the objective is to evaluate the state estimation localization and object re-identification from the KF, a sufficient number of observations  $s_{occ}$  is needed initially for the target before the occlusion so that the KF can capture the target object’s state. Furthermore, the length of occlusion  $l_{occ}$ , the number of detections excluded from the input, should also be determined. Thus, eligible objects for occlusion simulation should have  $n$  number of observations (detections) such that  $n \geq s_{occ} + l_{occ}$ .

In this experiment, the KITTI dataset is used with Virconv [26] detections,  $D$ , to satisfy the constraint on the number of observations for objects. Initially, the ground truth is used to match detections with objects in the ground truth. Next, objects with observations that satisfy the number of observation conditions  $D_{satisfy} \subseteq D, n \geq s_{occ} + l_{occ}$ , are collected for occlusion simulation, and the other detections  $D_{not.satisfy} \subseteq D$  are excluded. Two types of occlusions have been simulated in this experiment: mid-occlusions and late occlusions. Mid occlusions happen in the middle of an object’s trajectory, so the object reappears after the occlusion period ends. On the other hand, late occlusions occur at the end of an object’s trajectory, so the object will not reappear after the occlusion because it has left the sensor’s field of view. Even though both occlusion types can be used to evaluate state estimation for objects, mid-occlusions can assess the re-identification of objects after the occlusion period. Late occlusion simulates off-scene objects.

Given observations (detections) of the collected objects  $D_{satisfy}$  that satisfy the occlusion simulation condition,  $l_{occ}$  consecutive detections have been removed from these objects based on the type of occlusion (Mid/Late). The detection removal is done at the middle or the end of the trajectory of the objects after passing  $s_{occ}$  detections necessary for KF state estimation, as discussed earlier. Eventually, the remaining detections are combined with the rest of the detections,  $D_{not.satisfy}$ , to form the final detections that simulate the target occlusion, either mid- or late-occlusion.

#### 5.3.2 Occluded Targets Tracking and Re-Identification Evaluation

Table 5 shows a track evaluation of the simulated occlusions on the KITTI dataset with 10 and 20 consecutive frame occlusion periods. The experiment includes mid and late occlusion with at least 35 initial observations ( $s_{occ}$ ) before the occlusions. HOTA and MOTA metrics are used to evaluate tracking performance. In contrast, the IDF1 metric measures the success rate of re-identifying objects, including occluded ones. The proposed KF with motion dynamics outperforms the baseline KF in all metrics, with a margin of 1.24% in HOTA and 1.49% in MOTA with occlusion of length 20 frames. Moreover, the proposed KF improves object re-identification by 1.47% in IDF1 across frames. The difference in performance between the proposed KF and the baseline increases as the occlusion length increases in both mid and late occlusion, reflecting the advantage of the proposed KF in handling long occlusions.

Table 5: Performance comparison between the proposed method and the baseline Kalman filter in simulated occlusion scenarios with occlusion periods of ten and twenty frames with the jerk motion model on the KITTI dataset.

Occlusion Scenario		Method	HOTA (%)	MOTA (%)	IDF1 (%)
Exit-track Occlusion					
Type	Length ( $l_{occ}$ )				
Late	10	Baseline	81.01%	83.85%	91.04%
		Ours	<b>81.68%</b>	<b>84.72%</b>	<b>91.48%</b>
		Improvement	+0.67%	+0.87%	+0.44%
Late	20	Baseline	75.60%	76.56%	87.13%
		Ours	<b>76.84%</b>	<b>78.05%</b>	<b>87.92%</b>
		Improvement	+1.24%	+1.49%	+0.79%
Mid-track Occlusion					
Mid	10	Baseline	76.44%	78.20%	86.62%
		Ours	<b>77.32%</b>	<b>79.07%</b>	<b>86.97%</b>
		Improvement	+0.88%	+0.87%	+0.35%
Mid	20	Baseline	65.83%	67.38%	74.74%
		Ours	<b>67.05%</b>	<b>68.93%</b>	<b>76.21%</b>
		Improvement	+1.22%	+1.55%	+1.47%



## 6 Conclusion

This work presents a novel formulation of the Kalman filter that incorporates the motion dynamics of tracked objects, aiming to capture complex motion patterns. In contrast, the traditional Kalman filter relies on a constant motion model commonly referenced in the literature. The proposed Kalman filter with motion dynamics demonstrates improved state estimation and localization for occluded objects, enhancing their trajectory tracking compared to the baseline Kalman filter. Additionally, the integration of motion dynamics provides a substantial boost in tracking performance, surpassing recent KITTI and WOD benchmarks, and demonstrating versatility across various detectors. To address the limited evaluation of multi-object tracking methods (MOT) in public datasets due to the scarcity of annotated occlusion scenarios, this study introduces a strategy for simulating occlusion scenarios on these datasets with controlled occlusion lengths, enabling a thorough evaluation of MOT methods. The proposed Kalman filter shows remarkable improvements over the traditional Kalman filter in managing long occlusions, achieving tracking performance gains of 1.22% in HOTA and 1.55% in MOTA on the KITTI dataset. Moreover, implementing the proposed Kalman filter with motion dynamics is an efficient approach. It has an additional processing time per frame that does not exceed 0.083 ms, making it suitable for real-time applications.

## References

- [1] Mohamed Nagy, Naoufel Werghi, Bilal Hassan, Jorge Dias, and Majid Khonji. Robmot: Robust 3d multi-object tracking by observational noise and state estimation drift mitigation on lidar pointcloud, 2024.
- [2] Andreas Geiger, Philip Lenz, and Raquel Urtasun. Are we ready for autonomous driving? the kitti vision benchmark suite. In *Conference on Computer Vision and Pattern Recognition (CVPR)*, 2012.
- [3] Liu Yan-Chang and Zuo Xian-Gang. A maneuvering target tracking algorithm based on the interacting multiple models. *TELKOMNIKA Indonesian Journal of Electrical Engineering*, 11(7):3997–4003, 2013.
- [4] Ki-In Na, Sunglok Choi, and Jong-Hwan Kim. Adaptive target tracking with interacting heterogeneous motion models. *IEEE Transactions on Intelligent Transportation Systems*, 23(11):21301–21313, 2022.
- [5] Mohamed Nagy, Majid Khonji, Jorge Dias, and Sajid Javed. Dfr-fastmot: Detection failure resistant tracker for fast multi-object tracking based on sensor fusion. In *2023 IEEE International Conference on Robotics and Automation (ICRA)*, pages 827–833, 2023.
- [6] Wu et al. 3d multi-object tracking in point clouds based on prediction confidence-guided data association. *IEEE Transactions on Intelligent Transportation Systems*, 2022.
- [7] Ziming Zhu, Jiahao Nie, Han Wu, Zhiwei He, and Mingyu Gao. Msa-mot: Multi-stage association for 3d multimodality multi-object tracking. *Sensors*, 22(22):8650, 2022.
- [8] Jiawei He, Chunyun Fu, Xiyang Wang, and Jianwen Wang. 3d multi-object tracking based on informatic divergence-guided data association. *Signal Processing*, 222:109544, 2024.
- [9] Andreas Reich and Hans-Joachim Wuensche. Monocular 3d multi-object tracking with an ekf approach for long-term stable tracks. In *2021 IEEE 24th International Conference on Information Fusion (FUSION)*, pages 1–7, 2021.
- [10] Leichen Wang, Jiadi Zhang, Pei Cai, and Xinrun Lil. Towards robust reference system for autonomous driving: Rethinking 3d mot. In *2023 IEEE International Conference on Robotics and Automation (ICRA)*, pages 8319–8325, 2023.
- [11] Xinshuo Weng, Jianren Wang, David Held, and Kris Kitani. 3d multi-object tracking: A baseline and new evaluation metrics. *2020 IEEE/RSJ International Conference on Intelligent Robots and Systems (IROS)*, pages 10359–10366, 2019.
- [12] Qitai Wang, Yuntao Chen, Ziqi Pang, Naiyan Wang, and Zhaoxiang Zhang. Immortal tracker: Tracklet never dies. *arXiv preprint arXiv:2111.13672*, 2021.
- [13] Ziqi Pang, Zhichao Li, and Naiyan Wang. Simpletrack: Understanding and rethinking 3d multi-object tracking. In *ECCV Workshops*, 2021.
- [14] Aleksandr Kim, Aljoša Ošep, and Laura Leal-Taixé. Eagermot: 3d multi-object tracking via sensor fusion. In *2021 IEEE International Conference on Robotics and Automation (ICRA)*, pages 11315–11321, 2021.
- [15] Samuel Scheidegger, Joachim Benjaminsson, Emil Rosenberg, Amrit Krishnan, and Karl Granström. Mono-camera 3d multi-object tracking using deep learning detections and pmbm filtering. In *2018 IEEE Intelligent Vehicles Symposium (IV)*, pages 433–440. IEEE, 2018.

- [16] Depanshu Sani, Anirudh Iyer, Prakhar Rai, Saket Anand, Anuj Srivastava, and Kaushik Kalyanaraman. Sensor-agnostic graph-aware kalman filter for multi-modal multi-object tracking. In *International Conference on Pattern Recognition*, pages 380–398. Springer, 2024.
- [17] Pei Sun, Henrik Kretzschmar, Xerxes Dotiwalla, Aurélien Chouard, Vijaysai Patnaik, Paul Tsui, James Guo, Yin Zhou, Yuning Chai, Benjamin Caine, Vijay Vasudevan, Wei Han, Jiquan Ngiam, Hang Zhao, Aleksei Timofeev, Scott Ettinger, Maxim Krivokon, Amy Gao, Aditya Joshi, Yu Zhang, Jonathon Shlens, Zhifeng Chen, and Dragomir Anguelov. Scalability in perception for autonomous driving: Waymo open dataset. In *2020 IEEE/CVF Conference on Computer Vision and Pattern Recognition (CVPR)*, pages 2443–2451, 2020.
- [18] Nicola Marinello, Marc Proesmans, and Luc Van Gool. Triplettrack: 3d object tracking using triplet embeddings and lstm. In *Proceedings of the IEEE/CVF Conference on Computer Vision and Pattern Recognition*, pages 4500–4510, 2022.
- [19] Aleksandr Kim, Guillem Brasó, Aljoša Ošep, and Laura Leal-Taixé. Polarmot: How far can geometric relations take us in 3d multi-object tracking? In Shai Avidan, Gabriel Brostow, Moustapha Cissé, Giovanni Maria Farinella, and Tal Hassner, editors, *Computer Vision – ECCV 2022*, pages 41–58, Cham, 2022. Springer Nature Switzerland.
- [20] Xiyang Wang, Chunyun Fu, Zhankun Li, Ying Lai, and Jiawei He. Deepfusionmot: A 3d multi-object tracking framework based on camera-lidar fusion with deep association. *IEEE Robotics and Automation Letters*, 7(3):8260–8267, 2022.
- [21] Hai Wu, Wenkai Han, Chenglu Wen, Xin Li, and Cheng Wang. 3d multi-object tracking in point clouds based on prediction confidence-guided data association. *IEEE Transactions on Intelligent Transportation Systems*, 23(6):5668–5677, 2022.
- [22] Xiangyang Wu, Yiming Sun, Liangjian He, Wei Li, Yifan Wu, Mingqiang Ding, Changhu Lu, and Ping Li. Virtual sparse convolution for multimodal 3d object detection. [https://openaccess.thecvf.com/content/CVPR2023/supplemental/Wu\\_Virtual\\_Sparse\\_Convolution\\_CVPR\\_2023\\_supplemental.pdf](https://openaccess.thecvf.com/content/CVPR2023/supplemental/Wu_Virtual_Sparse_Convolution_CVPR_2023_supplemental.pdf), 2023. Supplemental Material, CVPR 2023.
- [23] Shaoshuai Shi, Chaoxu Guo, Li Jiang, Zhe Wang, Jianping Shi, Xiaogang Wang, and Hongsheng Li. Pv-rcnn: Point-voxel feature set abstraction for 3d object detection. In *Proceedings of the IEEE/CVF Conference on Computer Vision and Pattern Recognition (CVPR)*, June 2020.
- [24] Shaoshuai Shi, Xiaogang Wang, and Hongsheng Li. Pointtrcnn: 3d object proposal generation and detection from point cloud. In *The IEEE Conference on Computer Vision and Pattern Recognition (CVPR)*, June 2019.
- [25] Yan Yan, Yuxing Mao, and Bo Li. Second: Sparsely embedded convolutional detection. *Sensors*, 18(10):3337, 2018.
- [26] Wu et al. Virtual sparse convolution for multimodal 3d object detection. In *Proceedings of the IEEE/CVF Conference on Computer Vision and Pattern Recognition (CVPR)*, June 2023.
- [27] Wu et al. Casa: A cascade attention network for 3-d object detection from lidar point clouds. *IEEE Transactions on Geoscience and Remote Sensing*, 2022.
- [28] Lue Fan, Yuxue Yang, Yiming Mao, Feng Wang, Yuntao Chen, Naiyan Wang, and Zhaoxiang Zhang. Once detected, never lost: Surpassing human performance in offline lidar based 3d object detection. In *Proceedings of the IEEE/CVF International Conference on Computer Vision (ICCV)*, pages 19820–19829, 2023.